Using Diffusion Monte Carlo to Evaluate the Initial Conditions for Classical Studies of the Photodissociation Dynamics of HCl Dimer

Benjamin M. Auer and Anne B. McCoy*

Department of Chemistry, The Ohio State University, Columbus, Ohio 43210

Received: August 7, 2002

An approach for evaluating the initial conditions for classical studies of the photodissociation dynamics of molecular clusters is described. This approach is based on an approximate separation of the momentum and coordinate space probability distributions, evaluated using a wave function that is obtained from a Diffusion Monte Carlo simulation. Using the initial conditions that are generated by this approach, the photodissociation dynamics of HCl dimer is studied. Excellent agreement between the calculated and experimental angular momentum and vibrational energy distributions for the remaining HCl molecule and the kinetic energy distribution of the dissociated hydrogen atom are obtained. The kinetic energy distribution for the chlorine atom and angular distributions of the remaining hydrogen and chlorine atoms are also obtained and dynamical information contained in these distributions is discussed.

Introduction

Over the past several years there has been increased interest in photoinduced processes in molecular clusters.[1−11] The motivation for this work comes primarily from the belief that if one can photoinitiate a chemical reaction by exciting a molecule in a molecular cluster either vibrationally[4,5] or electronically,[1,2,6−8,10,11] one can gain insights into the dynamics of the underlying bimolecular reaction. Since the formation of a hydrogen- or van der Waals bond between the constituent molecules affects the bonding within each of the molecules (as is illustrated in the shifts of the intramolecular vibrational frequencies), initiating a reaction inside a cluster can alter the energetics of the reaction. Studies of how this affects the dynamics can provide insights into the effects of environment on the underlying reaction dynamics. Further, by studying photoinitiated processes within weakly bound complexes, one gains control over the relative orientations of the molecules prior to the reaction. This control cannot be achieved in the corresponding bimolecular process. Finally, by preparing the cluster with intermolecular vibrations excited, one can investigate how the resulting changes in the geometries that are sampled by the cluster affect the reactivity and reaction products, thereby providing insights into the coordinates along which the reaction occurs.[4]

While such studies are potentially very powerful, studies of UV photolysis of neutral clusters introduce several experimental challenges. These come from difficulties in finding experimental conditions that ensure that the complexes that are being studied are of the desired composition and that the observed reaction products are resulting from the reaction of interest and not other processes that are also occurring in the system. Further, the large number of atoms and possible reaction channels can make direct analysis of the dynamics, based on experimental observables, difficult. Therefore, to unravel the underlying dynamics from the experimental observations, it is often useful to perform simulations of the reaction of interest, since here one has complete control over the size of the system that is being studied, and the results of the simulations can be translated into a series of images that illustrate the time evolution of the dynamics.

In principle, this should be straightforward, assuming one has an appropriate model for the potential surface that describes the system of interest. In practice, there are some significant theoretical and computational hurdles that need to be addressed. Previous studies have demonstrated that classical mechanics can provide a realistic description of prompt UV photodissociation processes[12−14] and studies of vibrational predissociation in clusters.[15] In the case of the vibrational predissociation, the lifetimes of the resonance states to which the high frequency intramolecular vibration is excited are tens of picoseconds or longer. On these time scales, the system has enough time to lose memory of the initial conditions in the intermolecular degrees of freedom, and, as long as the correct total energy is contained in the cluster, the results are expected to be relatively insensitive to the details of the initial conditions.

In contrast, for prompt photodissociation, a reflection principle dominates the product state distributions. In other words, the disposal of energy among the various degrees of freedom reflects the initial conditions for the classical trajectories. Recently Jungwirth and co-workers showed that in classical studies of the photodissociation of HX (where X is Cl, Br, or I) in argon clusters a correct quantum mechanical sampling of the initial conditions for their simulations is crucial if quantitative agreement between experiment and theory is to be achieved.[12,16] We found that a similar reflection principle holds for energy transfer in collision induced dissociation of weakly interacting species.[17] Here, the amount of kinetic energy that is lost by the colliding atom can be related to the phase of the intermolecular vibration at the time of the collision. This effect is most pronounced when the collisions are geometrically constrained, as is the case for photoinduced processes in clusters.

To unravel the dynamics of photoinitiated processes in weakly bound complexes, we need an efficient approach for generating initial coordinate and momentum space distributions that reflect the quantum nature of the inter- as well as the intramolecular

* To whom correspondence should be addressed. E-mail: mccoy@chemistry.ohio-state.edu. Address: Department of Chemistry, The Ohio State University, Columbus, OH 43210.

10.1021/jp021826l CCC: $25.00 © 2003 American Chemical Society
Published on Web 12/03/2002

TABLE 1: Parameters Used to Define the Potential Surfaces for $(HCl)_2$

parameter	value
D_e/cm^{-1}	37 240.87
$\alpha/Å^{-1}$	0.52309
$r_e/Å$	1.274
A/cm^{-1}	514 615
$\beta/Å^{-1}$	2.2181

vibrations. This is nontrivial for weakly bound clusters. Unlike more strongly bound species, for which the ground state is well approximated by a *n*-dimensional Gaussian, harmonic approximations to the vibrational motions are not appropriate as the intermolecular vibrations are extremely anharmonic.

The remainder of this paper is divided into two parts. In the first, we focus on applications of diffusion Monte Carlo approaches for generating initial phase space distributions for classical simulations of direct photodissociation in weakly bonded clusters. In the second part of the paper, we apply these approaches to a study of the photodissociation dynamics of HCl dimer. Through comparisons between experiment and theory, we investigate the dynamics that underly the product state distributions that were observed by Valentini, Wittig, Kasai, and their co-workers.[7,8,10,11]

System

In this study, we focus on the photodissociation of HCl dimer. The HCl dimer has been the subject of a variety of experimental and theoretical studies including studies of the spectroscopy in the microwave and infrared,[18−21] studies of vibrational predissociation[22,23] and UV photodissociation.[7,8,10,11,13] The reason for our original interest in this system came from the fact that it is among the simplest molecular complexes, containing only four atoms, for which the potential surfaces are well characterized by other spectroscopic and dynamical studies and for which the UV photodissociation of a monomer is in an experimentally obtainable region of the electromagnetic spectrum. Since that time, UV photolysis of HCl dimer has been studied by Wittig, Kasai, and Valentini and their co-workers.[7,8,10,11]

In this work, we need to consider the dynamics of HCl dimer on two potential surfaces. Initially, the system is described by the ground-state wave function on the lowest energy electronic state. Once the dimer absorbs a UV photon, one of the two HCl bonds is broken and the potential can be approximated by the interaction of a hydrogen atom, a chlorine atom and a HCl molecule.

In describing the ground-state properties of $(HCl)_2$, the large frequency difference between the inter- and intramolecular degrees of freedom introduces a natural separation of the vibrational motions into two high-frequency HCl stretches, r_1 and r_2, and the four low-frequency intermolecular vibrations. The two HCl stretches are modeled by one-dimensional Morse functions,

$$V(r_i) = D_e[1 - e^{-\alpha(r_i - r_e)}]^2 \qquad (1)$$

where the parameters are given in Table 1. The intermolecular vibrations require four coordinates, illustrated in Figure 1. These are the usual Jacobi coordinates and are given by *R*, the distance between the centers of mass of the two monomers, θ_1 and θ_2 are the angles between the two HCl bonds and *R*, and ϕ is the angle between the plane that contains *R* and r_1 and the plane containing *R* and r_2. For simplicity, we assume that the intermolecular axis *R* lies along the *z*-axis and r_1 is in the *xz* plane. In this work, we use the potential of Elrod and Saykally.[18]

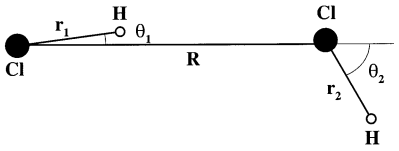

Figure 1. The coordinates used to describe the ground state of $(HCl)_2$.

Based on this surface, the dimer is bound by 692 cm^{-1}, the equilibrium structure has $R = 3.746$ Å, $\theta_1 = 9°$, $\theta_2 = 89.8°$, and $\phi = 180°$. The symmetry of the complex implies there is a second equivalent minimum in which $\theta_1 = 90.2°$ and $\theta_2 = 171°$ and the barrier between the two minima is 45 cm^{-1} above the potential minimum. The ground-state wave function samples both minima and the experimental tunneling splitting in this system is 15.5 cm^{-1}.

To aid in the discussion that follows, we refer to the HCl molecule that lies more nearly parallel to ***R*** as the *hydrogen bonding* HCl while the other HCl molecule is referred to as the *free* HCl. While in classical mechanics, we can choose which of the two HCl bonds is broken, experimentally the two HCl bonds have equal absorption cross sections at 193 nm and the experimental product state distributions reflect linear combinations of the two monomers being broken. As such, in the present simulations we break each of the HCl monomers with equal probability.

Once a HCl molecule has absorbed a UV photon, the system can no longer be considered as two HCl molecules, but rather a hydrogen atom, a chlorine atom and a HCl molecule. Following our previous work on this system, we model the reactive potential as the sum of three interactions. The first is the interaction between the hydrogen and chlorine atoms. This potential is described by

$$V_{H,Cl}(r_1) = Ae^{-\beta r_1} \qquad (2)$$

in which the parameters have been fit to the ab initio points of Hirst and Guest[24] and are given in Table 1. The interaction between the hydrogen atom and the remaining HCl molecule is described by the global H+HCl reactive potential of Truhlar and co-workers.[25] Finally, the interaction between the chlorine atom and HCl molecule is given by a modified Ar−HCl potential[26] which has been described previously.[13] By employing the above sum of two-body potentials, the following channels are included in the simulation,

$$\begin{aligned} H + Cl + H'Cl'(v,j) &\rightarrow H + Cl + H'Cl'(v',j') \\ &\rightarrow Cl + HH' + Cl' \\ &\rightarrow H' + Cl + HCl'(v',j') \end{aligned}$$

while the possibility for HCl recombination or Cl_2 formation are not included in this model potential. Of the included channels, the first corresponds to elastic or inelastic scattering. Since there is nearly zero-probability for H_2 formation in these simulations, we will use the term reactive collisions to refer to those reactions that undergo hydrogen atom exchange.

Arguably, there are choices in the constituent surfaces that can be used in such a study. Since the dynamics is prompt, after 20 fs have elapsed the H−Cl distance exceeds 10 Å, and we expect that the most important contributions to the potential are the shape of the HCl repulsive potential and the H+HCl reactive surface.

Theoretical Approaches

As was mentioned above, photodissociation dynamics in clusters can be described by classical mechanics, but the initial

conditions for the classical trajectories need to reflect the quantum properties of the initial vibrational state of the system. The work of Heller[27,28] has shown us that for high frequency vibrational modes, such as a HCl stretch, a correct description of the photodissociation cross section requires a proper quantum mechanical description of the HCl vibration. In addition, on the basis of the relatively weak interactions of the two HCl molecules in the dimer, it is anticipated that the rotational and vibrational state distributions of the HCl that remains after photodissociation are strongly correlated to the HCl vibrational and bending motions in the dimer. This is an example of the reflection principle. On the basis of this analysis, we expect the results of the simulations to be particularly sensitive to how well the choice of the initial coordinates and momenta of the atoms mimic the corresponding quantum phase space distribution.

This leads to two theoretical and computational challenges. The first is the determination of the wave function that describes the initial quantum state of the system, while the second is to carry out the transformation of this wave function to a quantum phase space distribution.

For the intramolecular vibrations, the two HCl stretches, the wave functions are evaluated in a discrete variable representation (DVR),[29] using the potential given by eq 1. In the case of the intermolecular vibrations in HCl dimer, the wave function can be obtained using large basis set approaches.[19,30] On the other hand, generating the codes for these calculations and evaluating the wave functions are extremely demanding. Further, analogous calculations for systems with five or more atoms or more than two interacting molecules are close to or exceed the types of variational calculations of vibrational states that can be routinely performed.

To generate an approach that can be applied to studies of photodissociation of larger clusters or clusters containing larger molecules, we elect to use an approach that is based on rigid body diffusion Monte Carlo.[31] Previous studies have demonstrated that this approach can be easily extended to studies of vibrational motions in quite large systems without a significant investment in the generation of new computer programs or in computer time.[32−36]

A. Diffusion Monte Carlo. Diffusion Monte Carlo (DMC) provides a way to determine the ground-state wave function for the system of interest using a Monte Carlo simulation. Our implementation is based on the work of Anderson,[37−39] of Suhm and Watts,[33] and of Buch.[31] A good review of the basic ideas behind DMC can be found in ref 33. Details of our approaches have been described previously,[32,40] and we provide a brief summary in order to have the terms necessary to describe the extensions needed to develop quantum phase space distributions from the DMC wave function.

In DMC, the ground-state wave function is obtained by solving the time-dependent Schrödinger Equation in an imaginary time variable $\tau = it$. For an arbitrary trial wave function that has a nonzero overlap with the vibrational ground state of the system of interest, it is well-known that

$$|\Psi(\tau)\rangle = \mathrm{e}^{-\hat{H}\tau/\hbar}|\Psi(\tau=0)\rangle = \sum_{n=0} \mathrm{e}^{-E_n\tau/\hbar}|\phi_n\rangle \qquad (3)$$

and

$$\lim_{\tau\to\infty} |\Psi(\tau)\rangle \to \mathrm{e}^{-E_0\tau/\hbar}|\phi_0\rangle \qquad (4)$$

where E_0 is the ground-state energy and $|\phi_0\rangle$ represents the lowest energy eigenstate of $\hat{H}$. In contrast to most other approaches that are commonly used to represent the wave function, in DMC, the wave function is represented by an ensemble of replicas of the system, or walkers, each of which is localized in the configuration space of the system. By assuming that each walker moves independently

$$\begin{aligned}|\Psi(\tau+\Delta\tau)\rangle &= \mathrm{e}^{-(\hat{H}-E_{\mathrm{ref}})\Delta\tau/\hbar}|\Psi(\tau)\rangle \\ &\approx \mathrm{e}^{-(\hat{V}-E_{ref})\Delta\tau/\hbar}\mathrm{e}^{-\hat{T}\Delta\tau/\hbar}|\Psi(\tau)\rangle \\ &\approx \sum_j \mathrm{e}^{-(\hat{V}-E_{\mathrm{ref}})\Delta\tau/\hbar}\mathrm{e}^{-\hat{T}\Delta\tau/\hbar}|\omega_j(\tau)\rangle \end{aligned} \qquad (5)$$

Here, $|\omega_j(\tau)\rangle$ represents the configuration and relative weight of the jth walker and E_{ref} provides an approximation to the zero-point energy of the system. E_{ref} is determined from the constraint that the magnitude $|\Psi(\tau)\rangle$ remains constant, or alternatively, the sum of the weights of the walkers is constant.[38]

Equation 6 is essentially the split operator propagator, introduced by Feit and Fleck[41] for quantum dynamics simulations. It provides an accurate approximation to the full propagator so long as $\Delta\tau$ is sufficiently small. This division of the operator allows us to divide the propagation of the walkers into two steps. In the first, the kinetic part of the Hamiltonian acts on the walker. This causes the position of the walker to be shifted by an amount that is taken from a Gauss-Random distribution, with a width in each Cartesian coordinate of $(\Delta x_i)^2 = \hbar\Delta\tau/m_i$ where m_i is the mass of the ith atom. The potential part of the propagator is purely multiplicative and multiplies the weight of the jth walker by $\exp\{-[V(\mathbf{r}_j) - E_{\mathrm{ref}}]\Delta\tau/\hbar\}$ where $\mathbf{r}_j$ represents the coordinates of the jth walker at time τ. Although there are several ways to motivate the approach, from a split operator formulation or from solving a diffusion equation, the resulting equations are identical.

Because our treatment of HCl dimer (or any other cluster) focuses only on the intermolecular degrees of freedom, a minor modification to the above procedure is made. Instead of allowing all of the atoms to move in their three Cartesian coordinates, only the centers of mass of the atoms are allowed to diffuse, while each molecule is also allowed to undergo rotational diffusion. Buch[31] showed that this leads to only minor adjustments to the translational diffusion part of the simulation. Descriptions of our implementation of this procedure can be found in ref 32.

B. Quantum Phase Space Distributions. Once we have a wave function, we need to have a way to transform this function that only depends on the coordinates of the atoms to a probability distribution that is a function of the coordinates and conjugate momenta of each of the atoms. For wave functions that are written as functions of Cartesian coordinates, or coordinates that are linear combinations of Cartesian coordinates, e.g., normal mode coordinates, the Wigner function[28]

$$W(r,p) = \frac{1}{2\pi\hbar}\int_{-\infty}^{\infty} \mathrm{d}s\, \mathrm{e}^{isp/\hbar}\Psi\left(q+\frac{s}{2}\right)\Psi^*\left(q-\frac{s}{2}\right) \qquad (6)$$

provides a function of the coordinates and momenta that is stable when propagated on the potential used to generate Ψ. This approach was taken to generate the initial conditions for the two intramolecular HCl stretches. In the case of the intermolecular degrees of freedom, two issues complicate this analysis. First, the wave function is expressed in terms of the orientations of the two HCl molecules and the distance between them and the above expression does not apply directly to wave functions that depend on angles. Second, while DMC provides an ensemble of walkers that represent the ground-state wave function, it does not give an analytical form for the wave

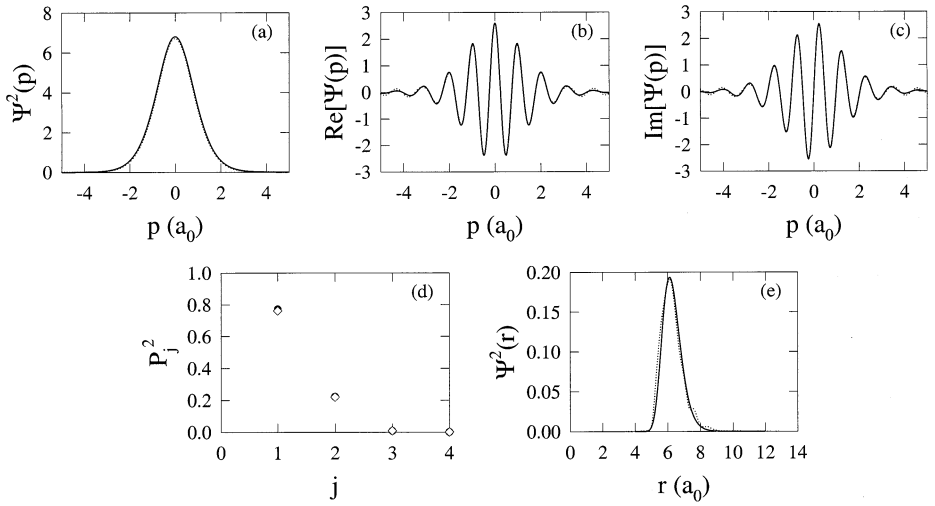

Figure 2. Comparison of DMC wave functions and probability distributions (dotted lines) and the corresponding results from variational calculations (solid) lines are plotted for the ground state of Ne_2 (a−c,e). In (d) we compare the projections of the ground-state wave function for a hindered rotor system onto angular momentum eigenstates, obtained by DMC (white diamonds) and from a converged variational calculation (black circles).

function from which $\Psi(q \pm s/2)$ can be readily evaluated. Consequently, we use an approximation to the Wigner distribution in which the phase space distribution is described by a product of the coordinate and momentum space probability distributions, taking into account of the fact that in angular degrees of freedom, when the magnitude of the projection of the angular momentum along **R** is $m\hbar$, the wave function must die to zero as $\sin^{|m|}(\theta_1)\sin^{|m|}(\theta_2)$.

Within this formulation of the phase space probability distribution, one still needs to find a way to evaluate the necessary functions when the form of the wave function is given by an ensemble of weighted points in space, where the weights provide the value of the wave function at that particular geometry of the cluster. As this is a Monte Carlo sampling of the ground-state wave function, we can use Monte Carlo integration[33,42] to evaluate the overlap integrals between the ground-state wave function, obtained by DMC, and the momentum eigenstates of interest. In the case of a one-dimensional vibrating system, this would require the evaluation of

$$\tilde{\Psi}(p) = \sqrt{\frac{1}{2\pi\hbar}} \int_{-\infty}^{\infty} \mathrm{d}x\, \mathrm{e}^{-ipx/\hbar} \Psi(x) \propto \sqrt{\frac{1}{2\pi\hbar}} \sum_{j=1}^{N_{\text{walkers}}} w_j \mathrm{e}^{-ipx_j/\hbar} \tag{7}$$

where the sum is over all of the walkers each of which has a position x_j and a weight w_j. To test this approach, we simulated the Ne−Ne stretch in neon dimer. In Figure 2a−c we compare the momentum space wave function, obtained by DMC, with the results obtained by numerically solving the Schrödinger equation and taking the Fourier transform of the result. Similarly, for rotational motions, we can project the wave function onto angular momentum eigenstates. Results of this approach for a one-dimensional hindered rotor are given in Figure 2d. As these results demonstrate, this approach provides a realistic depiction of the momentum space wave function and the corresponding probability distribution can be obtained by squaring the overlaps.

To obtain the corresponding coordinate space probability distribution we must take the overlap of the wave function with itself. This requires two, independent evaluations of the wave function at the positions of the walkers. One of these evaluations can be taken directly from the weights of the walkers at a particular time τ. For the second evaluation, we take advantage of the time reversal symmetry of the DMC simulation. Following Rothstein,[43] the ratio of the weight of the jth walker at time $\tau + \Delta\tau$ and the weight at time τ provides a second way to evaluate the value of the wave function at the coordinates of the j th walker at time τ. Multiplying these quantities together, we find that the value of the probability density at the coordinates of the jth walker at time τ is given by

$$\Psi^2(x_j(\tau)) = w_j(\tau) \times \frac{w_j(\tau + \Delta\tau)}{w_j(\tau)} = w_j(\tau + \Delta\tau) \tag{8}$$

and all that is required in order to obtain the probability density, rather than the value of the wave function at the coordinates of a particular walker, is a way to track how the weight of each of the walkers depends on time. We have found that a small number of time steps is sufficient to obtain stable results by this method. It should be noted that this approach is also closely related to the descendent weighting approach[33,44] which was proposed by Suhm and Watts for evaluating expectation values of an arbitrary multiplicative operator.

By repeating the above analysis for all of the walkers, the probability density can be obtained very easily. To illustrate the accuracy of this approach in Figure 2e we compare the variational and DMC probability distributions for the ground state of Ne_2.

C. Numerical Details. In the present study, we obtain the wave functions and phase space probability distributions for the two HCl stretching motions using a DVR scheme with 500 DVR points spaced from 0.74 to 2.6 Å along this coordinate. Then 5000 pairs of vibrational coordinates and momenta are chosen at random using an importance sampling scheme in which only those initial conditions that are larger than a random number between 0 and the maximum value of the Wigner function are used for the simulation. Since we are interested in UV photodissociation at 193 nm, we constrain the bond length of the HCl bond that is broken to be between 1.537 and 1.59 Å so that the energy difference between the ground and excited-state energy of the HCl is within 1000 cm^{-1} of the 193 nm photon.

To obtain the initial conditions for the intermolecular degrees of freedom, we perform a rigid body DMC simulation of the dimer using the potential of Elrod and Saykally[18] using the methods described above with 5800 walkers and a time step of 2.4 fs. The system is allowed to equilibrate over a million time steps, during which time each walker is given an equal weight

and walkers are added to or removed from the ensemble according to the procedures, described in ref 38. The distribution for Ψ^2 is obtained by propagating the simulation 10 time steps beyond the end point of the simulation. The positions of the walkers at the end of the simulation provide a list of configurations of the cluster from which the initial conditions for the simulations are drawn and the weights of each configuration are given by the values of Ψ^2 obtained from the simulation.

The initial conditions for the momenta are obtained within a partially separable approximation to the wave function. The distributions in P, the momentum conjugate to the HCl−HCl stretch coordinate, are obtained by projecting the DMC wave function onto the free particle momentum eigenstates. In these calculations, we neglect the angular dependence of the wave function. Likewise, the angular momentum dependence of the wave function is obtained by projecting the DMC wave function onto the coupled angular momentum basis,

$$\Phi j_1,j_2,m(\theta_1,\theta_2,\phi) = \mathrm{Y}_{j_1,m}(\theta_1,\phi)Y_{j_2,m}(\theta_2,0) \tag{9}$$

The above basis is identical to that used by Bacic, Saykally, and others in basis set calculations of HCl dimer.[18,19] As with the coordinate distributions, the value of the square of the momentum space wave function at a particular value of the linear and angular momenta contributes to the weight of the trajectory.

Once the lists of possible initial conditions are generated, 20000 sets of initial conditions are taken by randomly selecting values from the five lists. Each set of initial conditions is used for two trajectories, one in which the hydrogen bonding HCl bond is broken and one in which the free HCl bond is broken. Therefore, a total of 40 000 trajectories are run in this study.

Since the initial conditions are given in terms of the internal coordinates and their conjugate momenta, the first step is to transform these values into the corresponding Cartesian coordinates and momentum in which the dynamics are propagated. This is readily achieved for the three bond lengths, their conjugate momenta and the three angles. In the case of the angular momenta, we first transform from the total angular momentum of each monomer and the z-component into the corresponding angular velocities, using the relationships

$$J_i^2 = \hbar^2 j_i(j_i + 1) = \mu_i^2 r_i^4[\dot{\theta}_i^2 + \sin^2\theta_i\dot{\phi}_i^2] \tag{10}$$

$$J_{i,z} = m_i\hbar = \mu_i r_i^2 \sin^2\theta_i\dot{\phi}_i \tag{11}$$

where J_i^2 represents the total angular momentum of the ith HCl monomer, $J_{i,z}$ the z-component, j_i and m_i are the corresponding quantum numbers, and μ_i represents the reduced mass of the HCl molecule. It should be noted that since we embed the coordinate axis system so that $\boldsymbol{r}_1$ lies in the xz plane, the projection of its angular momentum onto the z-axis is zero and $m\hbar$ corresponds to the projection of the angular momentum of the second HCl monomer onto the complex-fixed z-axis. The above relationships can be inverted to give

$$\dot{\phi} = \frac{m\hbar}{\mu_2 r_2^2 \sin^2\theta_2} \tag{12}$$

$$\dot{\theta}_1 = \frac{\hbar\sqrt{j_1(j_1+1)}}{\mu_1 r_1^2} \tag{13}$$

$$\dot{\theta}_1 = \frac{\hbar}{\mu_2 r_2^2}\sqrt{j_2(j_2+1) - \frac{m^2}{\sin^2\theta_2}} \tag{14}$$

Focusing on eq 15, one finds that when $m \neq 0$ as $\theta_2 \rightarrow 0$, $\dot{\theta}_2$ becomes imaginary. This unphysical result arises from a kinetic coupling between the three internal angles and their conjugate momenta. Specifically, if m is nonzero, the complex cannot sample configurations in which one of the HCl molecules lies nearly parallel to the intermolecular axis. As such, these initial conditions lead to negative kinetic energy and are discarded. From the initial angles, distances and corresponding time derivatives, the initial Cartesian coordinates and momenta can be readily evaluated.

To summarize the above procedures, DMC is used to determine the initial coordinate and momentum space probability distributions and the initial conditions for the classical trajectories are sampled from a product of these two distributions, with the constraint that the initial conditions that lead to imaginary $\dot{\theta}_2$ are discarded as these correspond to unphysical configurations of the system in phase space. The probability distribution in coordinate space is a fully coupled function of the four intermolecular coordinates, while the momentum space distribution is expressed as a product of the distribution that depends on P_R and the one that depends on the three angular momentum quantum numbers.

Once an appropriate set of initial conditions is chosen, the classical dynamics is propagated using a Gear algorithm. To ensure that the system has reached the asymptotic region, the system is propagated for 60 fs after $r_1 + r_2 > 10.5$ Å and either the Cl−Cl distance exceeds 5.2 Å or the simulations has been run for more than 1.2 ps.

Before presenting the results of this study, it should be noted that in the study of the photodissociation dynamics of $(HCl)_2$, described in refs 13 and 45, DMC techniques were also used to obtain the initial conditions for classical studies of the dynamics. The approaches taken in the earlier work and in the present study differ in several important aspects. In the previous work, the DMC simulations were performed in the Cartesian coordinates of all of the atoms, whereas now DMC is applied to calculations of the energies and wave function of the intermolecular degrees of freedom. The approach taken in the earlier work leads to larger uncertainties due to the factor of 100 difference between the frequencies of the inter- and intramolecular vibrations. Despite the higher dimensionality of the DMC simulations in the earlier work, the wave function that was obtained from the DMC simulations was only used to determine the initial coordinates and momenta in the three angular degrees of freedom. The initial conditions in the radial degrees of freedom were obtained by evaluating a Wigner distribuiton function using a wave function that was obtained by using one-dimensional slices through the global surface, with all other degrees of freedom constrained to their equilibrium values. Finally, the initial coordinates for ϕ and its conjugate momentum were obtained independently of the initial conditions in θ_1 and θ_2 and their conjugate momenta. While this approach worked well for us at the time, it is neither as general nor as rigorous as the approach described above.

Results and Discussion

A. HCl Product State Distributions. To start, we will focus on the two features of the photodissociation of $(HCl)_2$ that were investigated by Valentini and co-workers,[8] specifically the HCl vibrational and angular momentum distributions following

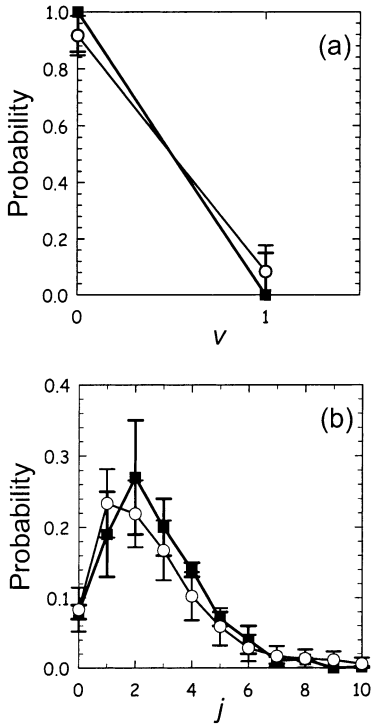

Figure 3. Plots of the final (a) vibrational and (b) angular momentum distributions of the HCl molecule that remains after photodissociation. The experimental distributions, reported by Valentini and co-workers, ref 8, are plotted with squares, while the calculated results are plotted with circles. The error bars on the calculated results represent one standard deviation, as defined in the text.

photodissociation of $(HCl)_2$ at 193 nm. These are plotted in Figure 3. In both cases, the distributions shown with black squares and thick error bars represent the experimental results, while the white circles, with thin error bars, provide the calculated results. The calculated vibrational energy distribution is obtained by taking the overlap of final values of r and p for the remaining HCl molecule with the Wigner distributions that correspond to each of the vibrational states. In other words, the relative probability that the HCl will end up in the state with vibrational quantum number n is given by

$$P_n = \frac{\sum_k w_k^{(i)} W_n(r_k(t_f),p_k(t_f))}{W_{tot}} \tag{15}$$

where the sum is over all of the trajectories, $w_k^{(i)}$ provides the weight of the kth trajectory, described above, $r_k(t_f)$ and $p_k(t_f)$ provide the HCl bond length and vibrational momentum at the end of the simulation, and $W_n(r,p)$ is the Wigner distribution, defined in eq 7 obtained from the nth eigenstate of HCl. We define W_{tot} to be the sum of the initial weights of all of the trajectories. The corresponding uncertainties are[46]

$$\sigma_n = \sqrt{\frac{W_{tot}\sum_k w_k^{(i)} W_n^2(r_k(t_f),p_k(t_f)) - [\sum_k w_k^{(i)} W_n(r_k(t_f),p_k(t_f))]^2}{W_{tot}^3}} \tag{16}$$

Once all of the P_n and σ_n have been calculated, they are normalized so that the P_n add up to one. As the results, plotted in Figure 3a, demonstrate the experimental and calculated results are in nearly exact agreement. The fact that both the experimental and calculated vibrational distributions show nearly 100% of the HCl is produced in $n = 0$ reflects the fact that the photodissociation is prompt and the HCl remains in the $n = 0$ vibrational state.

In the case of the angular momentum distributions, for each trajectory, we calculated the magnitude of the angular momentum of the remaining HCl molecule and assigned it to the closest integer multiple of $\hbar$. The plots are obtained by summing the weights of the trajectories that correspond to a particular value of j and normalizing the results so that the total probability is one. Here the uncertainties are obtained by[46]

$$\sigma_j = \sqrt{\frac{W_{tot}W_j - W_j^2}{W_{tot}^3}} \tag{17}$$

where

$$W_j = \sum_k{}' w_k^{(i)} \tag{18}$$

and the summation is only over those weights that correspond to trajectories for which the final angular momentum of the remaining HCl molecule, $j - 0.5 < j_f < j + 0.5$. The agreement between the experimental and calculated angular momentum distributions is also extremely good, and if we shift the calculated distribution to slightly larger j, nearly exact agreement would be achieved.

To further investigate the dynamics that lead to the observed HCl vibrational and angular momentum distributions, we divide the trajectories into two subsets, those for which the hydrogen bonding HCl monomer is broken and those in which the free HCl monomer is broken. The dimer undergoes large amplitude motions in θ_1 and θ_2, as is indicated by the 15.5 cm^{-1} tunneling splitting. As such, we define the hydrogen bonding HCl monomer to be the one for which $|\cos(\theta_i)|$ is closest to 1.

When the free HCl bond is broken, there is little interaction between the dissociating H and Cl atoms and the remaining HCl molecule. As a result, there is very little energy transferred to the remaining HCl molecule. This is illustrated by the fact that the average vibrational energy in the HCl bond is reduced by less than 0.2% for this subset of the trajectories. When we compare the initial and final angular momentum distributions for the remaining HCl, plotted in Figure 4, we find that they are nearly identical. The only notable difference is an increase in the angular momentum in those cases when the initial angular is zero. This shift is likely due to a small amount of energy transfer from the chlorine atom to the HCl molecule. Given the geometry of the complex and the smaller energy spacings between the $j = 0$ and $j = 1$ states of HCl, compared to the spacings between higher lying rotational levels and the vibrational levels, those states with $j = 0$ will be most sensitive to this small amount of energy transfer.

When we make similar comparisons between the initial and final angular momentum of the remaining HCl when the hydrogen bonding HCl bond is broken, the situation becomes more complicated. As is illustrated in Figure 5a,b, because the hydrogen bonding HCl is pointing toward the other HCl monomer when the HCl bond is broken, it is possible for the hydrogen to undergo either an inelastic or reactive collision with the remaining HCl monomer. Based on the trajectories, there is a 2% probability that a reaction will occur, while another 48% of the probability corresponds to trajectories that lead to a change in the internal energy of the remaining HCl monomer of more than 10%. This leads to an increase of the average vibrational energy of the remaining HCl monomer by ap-

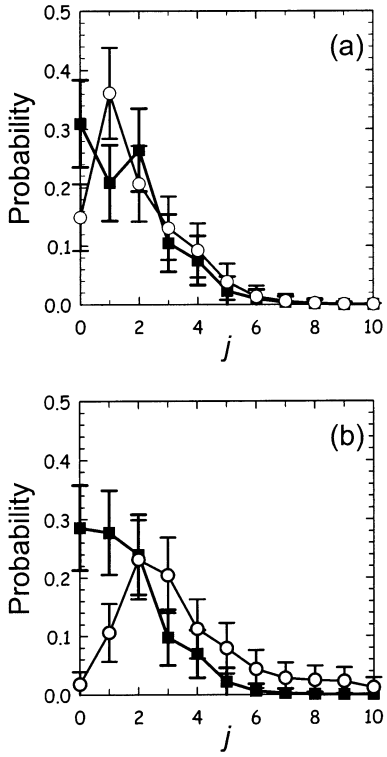

Figure 4. Plots of the angular momentum distributions at $t = 0$ (black squares) and at the end of the simulations (white circles) for (a) the hydrogen bonding HCl monomer when the free monomer bond is broken and (b) the free HCl monomer when the hydrogen bonding HCl bond is broken.

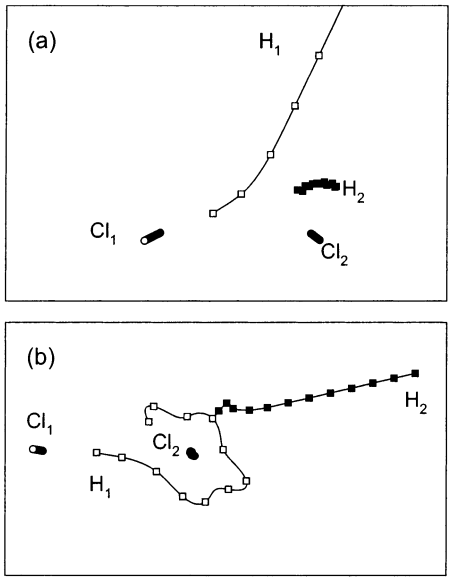

Figure 5. Representative trajectories are plotted for the cases when the hydrogen bonding HCl bond is broken. In both cases, the positions of the chlorine atoms are represented by circles and the hydrogen atoms are shown with squares. The positions of the four atoms are plotted every 12 fs.

proximately 35%. The resulting angular momentum distribution is shown in Figure 4b. The primary effects are a shift of the distribution and the long tail in the angular momentum distribution. In these calculations, we find that there are trajectories that lead to HCl products that have angular momenta as large as $j = 35$, although 99% of the trajectories have $j \leq 20$. In contrast, the initial wave function only contains nonzero j components with $j \leq 10$. The part of the angular momentum distribution of the remaining HCl molecule with $j \geq 5$ provides an experimental signature of trajectories in which there is energy transfer between the dissociated hydrogen atom and the remaining HCl molecule.

B. Chlorine and Hydrogen Atom Kinetic Energy and Angular Distributions. In a complementary set of studies, Wittig and co-workers[7] investigated the kinetic energy of the hydrogen atom that was released after the photodissociation of $(HCl)_2$. In contrast to the present study, in this experiment the free HCl molecule is vibrationally excited into the state with two quanta in the HCl stretch prior to photodissociation at 193.3 nm. As such, the free HCl bond is preferentially broken in this experiment. The most notable feature in the experimental hydrogen atom kinetic energy distribution is a series of peaks at energies above the translational energy that would be measured if the HCl monomer were allowed to dissociate in isolation. These peaks were attributed to vibrational states of the Cl−HCl complex.

In Figure 6a we plot the calculated kinetic energy distribution for the hydrogen atom. Focusing on the high energy tail of this distribution, shown in an enlarged scale in Figure 6c, we find that the distribution for the photodissociation of the free HCl monomer, plotted with a dotted line in Figure 6a,c, is in qualitative agreement with the experimental distributions, plotted in Figure 3 of ref 7. In their analysis, Wittig and co-workers attributed these features to transitions to bound states of the Cl−HCl complex. Since transitions to specific resonance states are purely quantum mechanical phenomena, we cannot expect to extract the peak structure from the classical results. On the other hand, we find that more than 10% of the trajectories display long-lived Cl−HCl complexes that undergo several vibrations prior to dissociation. These trajectories lead to the increased width of the hydrogen atom kinetic energy distribution, compared to the distribution that results from the photodissociation of the monomer, as can be seen by comparing the thick solid, dotted and dashed curves in Figure 6a,c. This feature of the dynamics also leads to the decrease in the kinetic energy of the chlorine atom, shown in Figure 6b,d.

Further investigation of the translational energy distributions of the hydrogen and chlorine atoms shows that there is a tail on the low energy side of the hydrogen atom translational distribution. This arises from energy transfer from the H atom into internal motions of the remaining HCl monomer. This comes from both inelastic scattering and reactive collisions. One feature that has been discussed in the context of photodissociation of HCl in argon clusters is the chattering of the hydrogen atom between the two heavy partners.[47] These collisions will lead to a tail in the chlorine kinetic energy distribution to higher energies. The fact that this peak extends only 500 cm^{-1} reflects the fact that there is rarely more than one collision between the hydrogen and chlorine atoms occurring after photodissociation.

Finally, we consider the angular distribution for the dissociating hydrogen and chlorine atoms in Figure 7. Since the transition moment is assumed to lie along the HCl bond that is broken, the angles that are used to plot the angular distributions in Figure 7 are defined to be the angles between the asymptotic velocity of the atoms and the orientation of the HCl molecule at $t = 0$. When the free HCl monomer is broken, there is little interaction between the hydrogen atom and the remaining ClHCl system. As a result the hydrogen atom angular distribution is narrow and peaked at $\theta = 0$. In contrast, the hydrogen atom angular distribution is much broader when the hydrogen bonding HCl monomer is broken. This shift results from both the inelastic and reactive collisions. In the case of the chlorine distributions,

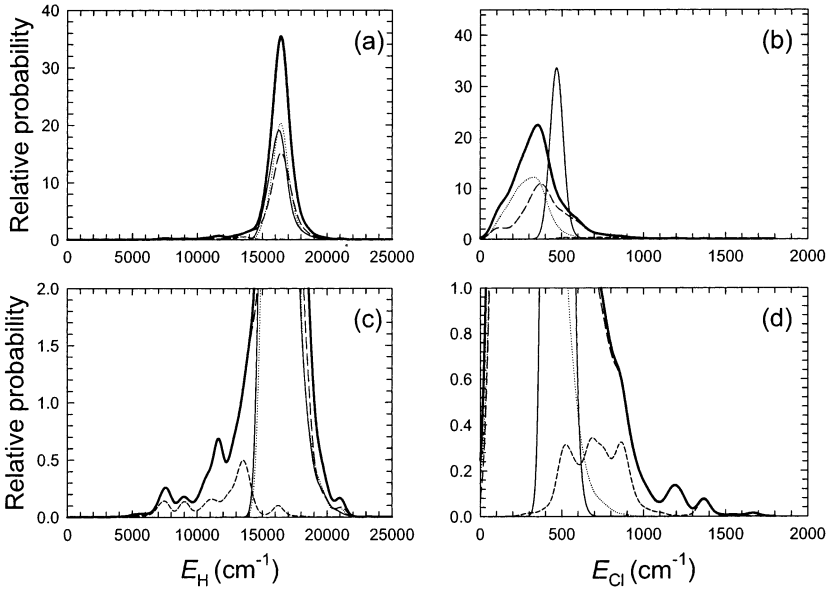

Figure 6. Plots of the kinetic energy distributions for the (a) hydrogen and (b) chlorine atoms. In all case, the full distribution is plotted in thick black lines. Dotted lines are used to show the fraction of the probability arising from the case when the free HCl monomer is broken, while long dashed lines are used to represent the case when the hydrogen bonding HCl bond is broken. Finally, the part of the kinetic energy distribution that results from reactive trajectories is plotted with short dashed lines. For comparison, the corresponding distributions that result when the second HCl molecule was not present are plotted with a thin solid line. In (c) and (d) we expanded the *y*-axis on (a) and (b) in order to make the small features more visible.

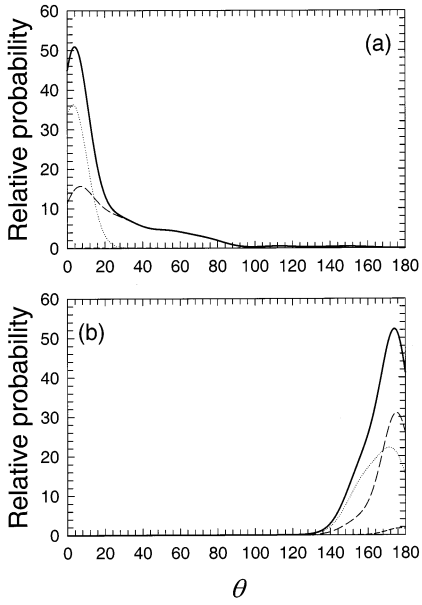

Figure 7. Plots of the angular distributions for the (a) hydrogen and (b) chlorine atoms. In all cases, the full distribution is plotted thick black lines. Dotted lines are used to show the fraction of the probability arising from the case when the free HCl monomer is broken, while long dashed lines are used to represent the case when the hydrogen bonding HCl bond is broken. Finally, the part of the kinetic energy distribution that results from reactive trajectories is plotted with short dashed lines.

the distributions are peaked at $\theta = \pi$. In contrast to the hydrogen atom angular distributions, the distribution when the free HCl monomer is dissociated is broader than the contribution from the dissociation of the hydrogen bonding HCl. This provides further evidence of the fact that the hydrogen atom does not undergo more than one or two collisions with the Cl atoms after the hydrogen bonding HCl bond is broken. In the case of the dissociation of the free HCl monomer, the formation of a Cl−HCl complex that can rotate prior to dissociation leads to the broadening of the angular distribution.

In contrast to the hydrogen atom kinetic energy distributions, neither the chlorine atom kinetic energy nor the angular distributions have been measured. Experimental studies of these properties would provide a measure of the energy transfer from the hydrogen atom to the other species in the complex, and through this additional information about the amplitude of the vibrational motions of the HCl monomers in the dimer. In the case of the angular distributions, differences between the measured distributions for the chlorine and hydrogen atoms would provide more information about the role of the Cl−HCl complex in these systems.

Summary and Conclusions

In this paper we described the results of our study of the photodissociation dynamics of $(HCl)_2$. In comparing the results of this work to those obtained experimentally, we find that the vibrational and angular momentum distributions for the HCl product are in excellent agreement. Since both of these distributions are found to closely resemble the motions of the two HCl molecules in the dimer, the good agreement between the experimental and calculated distributions provides a stringent test on the potential of Elrod and Saykally.[18] This agreement also helps further verify that the distributions that were reported by Valentini and co-workers result from the photodissociation of the dimer[8] and not from processes involving bimolecular reactions or larger clusters. Finally, the agreement also provides verification that the DMC based methods used to generate the initial phase space distributions for the classical trajectories provide an efficient and effective approach, at least for processes, like the present system, in which the dynamics is prompt.

We also investigated the final distributions for the chlorine and hydrogen atoms after the photodissociation. Again, the agreement with experiment is good,[7,10,11] but because the structures observed in the experiment correspond to quantized energy levels of the Cl−HCl complex only qualitative agreement can be achieved from classical studies of the dynamics. In addition, on the basis of an analysis of the connections between the dynamics and the calculated distributions, we believe that

analysis of the chlorine atom kinetic energy distribution and the angular distributions of the chlorine and hydrogen atoms would provide further insights into the nature of the Cl−HCl complex that is formed upon photodissociation. Further, analysis of the red tail on the kinetic energy distribution for the hydrogen as well as the angular distribution should provide information about the fraction of the complexes that are undergoing inelastic or reactive collisions, following photodissociation. This, in turn would provide valuable information about the transition state region of the H+HCl potential surface.

Acknowledgment. The authors gratefully acknowledges the National Science Foundation through grant number CHE-0200968, the donors to the Petroleum Research Fund administered by the American Chemical Society and the Dreyfus foundation awards program for partial support of this work. B.M.A. acknowledges The Dreyfus Foundation for a Jean Dreyfus Boissevain summer research scholarship and the College of Arts and sciences at Ohio State for an honors research scholarship support. Finally, we thank Professor Jim Valentini for encouraging us to revisit this system and for providing us with the experimental numbers, used in Figure 3.

References and Notes

(1) Wittig, C.; Sharpe, S.; Beaudet, R. A. *Acc. Chem. Res.* **1988**, *21*, 341−47.
(2) Scherer, N. F.; Khundkar, L. R.; Bernstein, R. R.; Zewail, A. H. *J. Chem. Phys.* **1987**, *87*, 1451−3.
(3) Wheeler, M. D.; Anderson, D. T.; Lester, M. I. *Int. Rev. Phys. Chem.* **2000**, *19*(4), 501−29.
(4) Lester, M. I.; Pond, B. V.; Anderson, D. T.; Anderson, L. B.; Wagner, A. F. *J. Chem. Phys.* **2000**, *113*(22), 9889−92.
(5) Chen, Y. L.; Heaven, M. C. *J. Chem. Phys.* **2000**, *112*(17), 7416−24.
(6) Zhang, J.; Dulligah, M.; Segall, J.; Wen, Y.; Wittig, C. *J. Phys. Chem.* **1995**, *99*(37), 13680−90.
(7) Liu, K.; Kolessov, A.; Partin, J. W.; Bezel, I.; Wittig, C. *Chem. Phys. Lett.* **1999**, *299*(5), 374−80.
(8) Picconatto, C. A.; Ni, H.; Srivastava, A.; Valentini, J. J. *J. Chem. Phys.* **2001**, *114*(16), 7073−80.
(9) Baumfalk, R.; Nahler, N. H.; Buck, U. *Faraday Discuss. Chem. Soc.* **2001**, *118*, 247−56.
(10) Imura, K.; Ohoyama, H.; Naaman, R.; Che, D.-C.; Hashinokuchi, M.; Kasai, T. *J. Mol. Struct.* **2000**, *552*, 137−45.
(11) Che, D.-C.; Hashinokuchi, M.; Shimizu, Y.; Ohoyama, H.; Kasai, T. *Phys. Chem. Chem. Phys.* **2001**, *3*(22), 4979−83.
(12) Slavíček, P.; Ždánská, P.; Jungwirth, P.; Baufalk, R.; Buck, U. *J. Phys. Chem. A* **2000**, *104*, 7793−802.
(13) McCoy, A. B.; Hurwitz, Y.; Gerber, R. B. *J. Phys. Chem.* **1993**, *97*, 12516−22.
(14) Segall, J.; Yen, Y.; Singer, R.; Wittig, C.; Garc×c1a-Vela, A.; Gerber, R. B. *Chem. Phys. Lett.* **1993**, *207*(4−6), 504−9.
(15) Miguel, B.; Bastida, A.; Zúñiga, J. Z.; Requena, A.; Halberstadt, N. *Faraday Discuss. Chem. Soc.* **2001**, *118*, 257−68.
(16) Ždánská, P.; Schmidt, B.; Jungwirth, P. *J. Chem. Phys.* **1999**, *110*(13), 6246−56.
(17) Lopez, J. G.; McCoy, A. B. In preparation.
(18) Elrod, M. J.; Saykally, R. J. *J. Chem. Phys.* **1995**, *103*, 933−49.
(19) Qiu, Y.; Bacic, Z. *J. Chem. Phys.* **1997**, *106*(6), 2158−70.
(20) Fàrnìk, M.; Davis, S.; Schuder, M. D.; Nesbitt, D. J. *J. Chem. Phys.* **2002**, *116*(14), 6132−45.
(21) Ohashi, N.; Pine, A. S. *J. Mol. Spectrosc.* **1984**, *81*(1), 73−84.
(22) Qiu, Y.; Zhang, J. Z. H.; Bacic, Z. *J. Chem. Phys.* **1998**, *108*(12), 4804−16.
(23) Ni, H.; Serafin, J. M.; Valentini, J. J. *J. Chem. Phys.* **2000**, *113*(8), 3055−66.
(24) Hirst, D. M.; Guest, M. F. *Mol. Phys.* **1980**, *41*, 1483.
(25) Schwenke, D. W.; Tucker, S. C.; Steckler, R.; Brown, F. B.; Lynch, G. C.; Truhlar, D. G.; Garrett, B. C. *J. Chem. Phys.* **1989**, *90*(6), 3110−20.
(26) Hutson, J. M. *J. Chem. Phys.* **1988**, *89*(8), 4550−57.
(27) Heller, E. J. *J. Chem. Phys.* **1978**, *68*(5), 2066−75.
(28) Brown, R. C.; Heller, E. J. *J. Chem. Phys.* **1981**, *75*(1), 186−8.
(29) Colbert, D. T.; Miller, W. H. *J. Chem. Phys.* **1992**, *96*(3), 1982−91.
(30) Wu, X. T.; Hayes, E. F.; McCoy, A. B. *J. Chem. Phys.* **1999**, *110*, 2365−75.
(31) V. Buch. *J. Chem. Phys.* **1992**, *97*, 726−29.
(32) Lee, H.-S.; Herbert, J. M.; McCoy, A. B. *J. Chem. Phys.* **1999**, *111*, 9203−12.
(33) Suhm, M. A.; Watts, R. O. *Phys. Rep.* **1991**, *204*, 293.
(34) Severson, M. W.; Buch, V. *J. Chem. Phys.* **1999**, *111*(24), 10866−75.
(35) Clary, D. C. *J. Chem. Phys.* **2001**, *114*(22), 9725−32.
(36) Quack, M.; Stohner, J.; Suhm, M. A. *J. Mol. Struct.* **2001**, *599*(1−3), 381−425.
(37) J. B. Anderson. *J. Chem. Phys.* **1975**, *63*, 1499−1503.
(38) J. B. Anderson. *J. Chem. Phys.* **1976**, *65*, 4121−27.
(39) J. B. Anderson. *Int. Rev. Phys. Chem.* **1995**, *14*, 85−112.
(40) Lee, H.-S.; Herbert, J. M.; McCoy, A. B. *J. Chem. Phys.* **1999**, *110*, 5481−4.
(41) Feit, M. D.; J. A. Fleck, J. *J. Chem. Phys.* **1983**, *71*(1), 301−8.
(42) Press: W. H.; Flannery, B. P.; Teukolsky, S. A.; Vetterling, W. T. *Numerical Recipies*; Cambridge University Press: New York, 1989.
(43) Langfelder, P.; Rothstein, S. M.; Vrbik, J. *J. Chem. Phys.* **1997**, *107*(20), 8526−35.
(44) Sandler, P.; oh Jung, J.; Szczesniak, M. M.; Buch, V. *J. Chem. Phys.* **1994**, *101*(2), 1378−91.
(45) McCoy, A. B.; Garcia-Vela, A.; Gerber, R. B. In *Ultrafast Reaction Dynamics and Solvent Effects*; Gauduel, Y., Rossky, P. J., Eds.; American Institute of Physics: New York, 1994; pp 516−27.
(46) Raff, L. M.; Thompson, D. L. *Theory of Chemical Reaction Dynamics*; CRC Press: Boca Raton, FL, 1985; Vol. III, Chapter 1, pp 1−121.
(47) Juanes-Marcos, J. C.; Garcia-Vela, A. *J. Chem. Phys.* **1999**, *111*(6), 2606−19.